Calcium-Activated Chloride Channels in Newly Differentiating Mouse Lens Fiber Cells and Their Role in Volume Regulation

Jun-Jie Tong, Pooja Acharya, and Lisa Ebihara

Department of Physiology and Biophysics, Rosalind Franklin University of Medicine and Science, Chicago, Illinois, United States

Correspondence: Lisa Ebihara, Department of Physiology and Biophysics, Rosalind Franklin University of Medicine and Science, 3333 Green Bay Road, Chicago, IL 60064, USA; lisa.ebihara@rosalindfranklin.edu.

Submitted: January 14, 2019
Accepted: March 14, 2019

Citation: Tong J-J, Acharya P, Ebihara L. Calcium-activated chloride channels in newly differentiating mouse lens fiber cells and their role in volume regulation. *Invest Ophthalmol Vis Sci*. 2019;60:1621–1629. https://doi.org/10.1167/iovs.19-26626

Purpose. Chloride channels have been proposed to play an important role in the regulation of lens volume. Unfortunately, little information is available about the molecular identity of these channels or how they are regulated in the lens due to the difficulties in isolating mouse fiber cells. Recently, our laboratory has developed a new technique for isolating these cells by using transgenic mouse lenses that lack both Cx50 and Cx46. The purpose of this study was to test the hypothesis that newly differentiating mouse fiber cells express calcium-activated chloride channels (CaCCs) by using this technique.

Methods. Differentiating fiber cells were isolated from lenses of double knockout mice that lack both Cx50 and Cx46 by using collagenase. Membrane currents were studied using the whole-cell patch clamp technique. The molecular identity and distribution of CaCCs were investigated using RT-PCR and immunofluorescence.

Results. Our electrophysiologic experiments suggest that peripheral fiber cells express a calcium-activated chloride current. The voltage gating properties, calcium sensitivity, and pharmacologic properties of this current resembled those of TMEM16 CaCCs. RT-PCR analysis demonstrated the presence of TMEM16A and TMEM16B transcripts in wild-type and double knockout mouse lenses. Both TMEM16A and TMEM16B proteins were detected in the differentiating epithelial cells and newly elongating fiber cells near the equator of the lens by immunohistochemistry.

Conclusions. Our results demonstrate that membrane conductance of peripheral fiber cells contain CaCCs that can be attributed to TMEM16A and TMEM16B. Given their critical role in volume regulation in other tissues, we speculate that these channels play a similar role in the lens.

Keywords: lens opacity, chloride channel, electrophysiology, volume regulation, intracellular calcium

The human lens is responsible for the fine focusing of both close and distant objects on the retina. To accomplish this task, the lens must be transparent and have a high index of refraction. It also has to be able to change its shape rapidly. During the process of aging, the lens gradually becomes stiffer and less transparent, leading to the development of presbyopia and cataracts, respectively.

There are no blood vessels in the lens. Thus, to maintain metabolic homeostasis and optical clarity, the lens must depend on a unique internal circulation system that consists of fluid fluxes flowing into the lens at the anterior and posterior poles and out of the lens at the equator. These fluid fluxes enable the transport of nutrients to the core of the lens and the removal of metabolic byproducts while maintaining lens steady-state volume and refractive properties. According to the fluid circulation system model proposed by Mathias (reviewed in Ref. 1), this internal circulatory system consists of continuously circulating ionic fluxes carried primarily by sodium that flow into the lens along the narrow extracellular spaces between the fiber cells. As sodium moves toward the center of the lens, it is continuously entering the fiber cells through sodium leak channels. Once inside the fiber cell, sodium flows from cell to cell via gap junctions moving toward the surface of the lens. The surface epithelial cells contain large numbers of Na^+-K^+ ATPases that then pump sodium out of the lens. It is hypothesized that the sodium flux is accompanied by the flow of water, which is driven through gap junctions by hydrostatic pressure from the center of the lens to the surface, where it flows out of the lens through aquaporins.[2]

Another element of this circulatory system involves chloride channels.[3] It has been shown that exposure of the lens to the chloride channel blocker NPPB under isotonic conditions results in an increase in lens volume and light scattering, suggesting that, under normal conditions, the lens fiber cells have a constitutively active chloride flux that plays an essential role in the regulation of lens volume and the maintenance of transparency.[4] The direction of this chloride flux is thought to be outward in the peripheral-most fiber cells and inward in the deeper layers of fiber cells, due to radial changes in the membrane potential of fiber cells relative to the extracellular space.[1]

Unfortunately, little information is available about the molecular identity of these chloride channels or how they are regulated in the lens. This is, in part, due to difficulties in

dissociating lens fiber cells for patch clamp recording. We have recently developed a new technique that makes electrophysiologic and imaging studies of these channels in dissociated lens fiber cells feasible.[5,6] This technique uses double knockout (KO) mice that lack both Cx50 and Cx46. The isolation of fiber cells from the lenses of these knockout mice can be accomplished using much milder dissociation conditions than those required in past attempts to study fiber cell activity, possibly due to alterations in cell adhesion properties.[7,8] Another advantage is that the double KO fiber cells can tolerate exposure to calcium-containing solutions.

Motivated by this discovery, we set out to test the hypothesis that mouse fiber cells functionally express calcium-activated chloride channels (CaCCs) that potentially play a role in volume regulation in the lens. Our results show that freshly dissociated peripheral fiber cells from double KO lenses express classical CaCCs whose electrophysiologic properties are generally consistent with those of TMEM16A (Anoctamin-1). In addition, we have characterized the expression of TMEM16A and TMEM16B transcripts and protein in the mouse lens by using RT-PCR and immunohistochemic techniques.

Methods

Chemicals

2-(4-chloro-2-methylphenoxy)-N-[(2-methoxyphenyl)methylideneamino]-acetamide (Ani9) was obtained from Tocris Bioscience (Bristol, UK). All other chemicals were purchased from Sigma-Aldrich Chemicals Company (St. Louis, MO, USA) or ThermoFisher Scientific unless otherwise specified.

For tissue harvesting, mice were euthanized and eyes were extracted using procedures approved by the Rosalind Franklin University Animal Care and Use Committee and in accordance with the ARVO Statement for the Use of Animals in Ophthalmic and Vision Research.

Mice

Transgenic Cx46(−/−) Cx50(−/−) double KO mice were generated as previously described.[5] Both wild-type and transgenic mice were in a C57 genetic background.

Dissociation of Differentiating Lens Fiber Cells

Fiber cells were dissociated from double KO mouse lenses as previously described.[6] Briefly, the capsule was removed from double KO mouse lenses and incubated in dissociation buffer (DB) containing 0.0625% collagenase (type IV; Worthington Biochemical, Lakewood, NJ, USA) and 0.025% protease (type XXIV; Sigma-Aldrich) at room temperature for 15 minutes. The capsule was washed once with DB and resuspended in DB. The epithelial and young fiber cells were then mechanically removed from the capsule by gentle trituration with a Pasteur pipette, pelleted (1,000 rpm for 2 minutes), and resuspended in DB. The isolated cells were used immediately for patch clamp experiments.

Patch Clamp Experiments

Membrane currents were recorded from isolated fiber cells by using the whole-cell patch clamp technique. A 60-mm tissue culture dish was used as the recording chamber. An Axoclamp 200B patch clamp amplifier (Molecular Devices, Sunnyvale, CA, USA) or MultiClamp 700A patch clamp amplifier (Molecular Devices) was used to control membrane potential and measure membrane current. The resistance of the patch pipettes was 2.5 to 4 MΩ when filled with standard internal solution. The composition of CsCl internal solutions used in most of the experiments is shown in Table 1. The final, free calcium concentration of the internal solution was calculated using EQCAL for Windows software (Biosoft, Cambridge, UK). The standard extracellular solution contained (in mM) 140 NaCl, 10 CsCl, 4.7 KCl, 1 $MgCl_2$, 1 $CaCl_2$, 5 glucose, and 5 HEPES, with pH adjusted to 7.4 with NaOH. Sodium gluconate external solution was prepared by substituting 140 mM sodium gluconate for equimolar NaCl in the bath solution. The N-methyl-D-glucamine chloride (NMDG-Cl) external solution contained (in mM) 150 NMDG-Cl, 4.7 KCl, 1 $MgCl_2$, and 1 $CaCl_2$. The patch pipette was positioned on the cell with a PatchStar micromanipulator (Scientifica, East Sussex, UK). Pulse generation and data acquisition were performed using a personal computer equipped with commercial software (PCLAMP 10; Molecular Devices) and a high-resolution, low-noise digitizer (Digidata 1440A or 1550B; Molecular Devices). The cell was focally perfused with drugs by using a gravity driven, millimanifold applicator (ALA Scientific, Farmingdale, NY, USA) whose tip was brought near and pointed at the cell of study using a manipulator. Solutions flowing over the cell could be changed within a few seconds by using this system. The bath was grounded via a 1-mm-diameter Ag/AgCl wire electrode mounted in a pipette tip filled with 3M KCl agar. Images of fiber cells were acquired via a cooled CCD camera (Coolsnap ES2, Photometrics; Roper Scientific, Tucson, AZ, USA) driven by an imaging program (Nikon Elements AR 4.60; Nikon Instruments, Melville, NY, USA). All the experiments were conducted at room temperature (21–24°C).

Table 1. Composition of CsCl Internal Solution

	$[Ca^{2+}]_I$ (nM)		
Compound	**0**	**0.2**	**0.6**
CsCl, mM	140	124	121.6
$CaCl_2$, mM	0	8.0	9.2
HEPES, mM	10	10	10
EGTA-Cs, mM	10	10	10
MgATP, mM	1	1	1
pH	7.4	7.4	7.4

For the ion selectivity experiments, the membrane potentials were corrected for liquid-junction potentials after the experiment using the "junction potential calculator" interface (Clampex version 10; Molecular Devices).

Data were analyzed using three different programs (PCLAMP 10 [Molecular Devices], SigmaPlot 11 [Systat Software, Chicago, IL, USA], and Origin 2017 [OriginLab, Northhampton, MA, USA]). Data points were reported as mean ± SEM unless otherwise indicated.

Immunohistochemistry

Eyeballs from 10- to 14 day-old wild-type mice were fixed with 4% paraformaldehyde in PBS (pH 7.4) at 4°C for 18 to 24 hours. Eyeballs were washed 3 times for 10 minutes with 1× PBS and incubated in 30% sucrose for 48 hours at 4°C. For sectioning, whole eyeballs were mounted in either an axial or equatorial orientation in a cryomold encased in optimum cutting temperature compound, and frozen on dry ice. Twenty-micrometer-thick sections were cut (Microm GmbH 69190, Walldorf, Germany) at −18°C by using disposable blades (Thermo Fisher Scientific) and transferred to Tissue Path Superfrost Plus Gold slides.

For immunostaining of TMEM16A and TMEM16B, antigen retrieval was performed by treatment of paraformaldehyde-fixed sections with 1% SDS in PBS at room temperature for 5

Investigative Ophthalmology & Visual Science

Table 2. Primer Pairs for CaCC mRNA

Target (Gene Name)	Accession No. (Amplified Region)	Primer Pair	Product Size, bp
TMEM16A (Ano1)	NM_178642.5 (471–829)	5′-accatcacaagagagcctcag-3′ 5′-cgtctcactgatgtggtaca-3′	359
TMEM16B (Ano2)	NM_153589.2 (633–881)	5′-gaggcgcacacctgggtcac-3′ 5′-atggggcgtggatccggaca-3′	249
β-Actin (Actb)	NM_007393.3 (28–246)	5′-cagcttctttgcagctcctt-3′ 5′-tcacccacataggagtcctt-3′	219

minutes, followed by 3 washes with 1× PBS. The sections were then processed for immunofluorescence using the Alexa Fluor 488 Tyramide SuperBoost Kit (ThermoFisher Scientific), as per the manufacturer's recommendations. The following primary antibodies and dilutions were used: rabbit polyclonal anti-TMEM16A (ab72984, dilution 1:100; Abcam, Cambridge, UK), rabbit polyclonal anti-TMEM16A (ab53212, dilution 1:100; Abcam), rabbit polyclonal anti-TMEM16A (PA5-77373, dilution 1:100; ThermoFisher Scientific), rabbit polyclonal anti-TMEM16B (PA5-77374, dilution 1:100; ThermoFisher Scientific). Rabbit isotype IgG (ThermoFisher Scientific) was used for negative control at a dilution of 1:100. Texas Red-conjugated wheat germ agglutinin (1:100 dilution; ThermoFisher Scientific) was used for labeling of cell membranes. 4′,6-diamidino-2-phenylindole (ThermoFisher Scientific) was used for fluorescent labeling of cell nuclei.

Confocal images were obtained using a laser scanning confocal fluorescent microscope (Fv10i Olympus, Waltham, MA, USA). Images were collected by sequential scanning using single laser-line excitation to eliminate bleeding from one channel into the other. Images were analyzed using Olympus software. Composite figures were assembled using Adobe Photoshop CS6 (Adobe Systems Inc., San Jose, CA, USA).

RNA Isolation and RT-PCR

Total lens RNA was isolated from four C57BL/6 mice and seven double KO mice by using the PureLink RNA Mini Kit (Invitrogen, Carlsbad, CA, USA). The extracted RNA was eluted in RNase-free water and incubated with TURBO DNase (Ambion, Austin, TX, USA) for 30 minutes followed by precipitation with lithium chloride to remove genomic DNA contamination. Complementary DNA synthesis reactions were performed with total RNA (1 μg) by using the LunaScrip RT SuperMix Kit (New England Biolabs, Ipswich, MA, USA), according to the manufacturer's instruction. The expression of TMEM16A, TMEM16B, and β-actin was determined using PCR. The cDNA samples were amplified using the GoTaqColorless PCR Master Mix Kit (Promega, Madison, WI, USA) on the Applied Biosystems 2720 Thermal Cycler (Forster City, CA, USA) with the strategy previously described by Kamikawa et al.[9] Briefly, cDNA (20 ng) and gene-specific primers pairs (Table 2) were added to a GoTaqColorless PCR Master Mix Kit and subjected to PCR amplification (1 cycle at 95°C for 2 minutes and 40 cycles at 95°C for 40 seconds, 55°C for 45 seconds, and 73°C 1 minute), followed by a dissociation stage (1 cycle at 73°C for 5 minutes). All PCR reactions were run in triplicates.

Results

Calcium-Activated Chloride Currents in Differentiating Epithelial and Fiber Cells Isolated from Mouse Lenses

Calcium-activated currents were studied in freshly isolated differentiating epithelial cells and fiber cells from double KO mouse lenses by using the whole-cell patch clamp technique. The cells had membrane capacitances ranging between 17.7 and 105.5 pF, corresponding to cell lengths between 22.8 and 389 μm, respectively. All of the cells had nuclei indicating that they were from the outer cortex. To block endogenous potassium currents, we substituted cesium for potassium in the internal solution and added 10 mM CsCl to the bath solution.

In cells dialyzed with internal solutions containing ≥200 nM $[Ca^{+2}]_i$, we observed the development of an outwardly rectifying current and associated inward tail current in response to voltage clamp ramps from –80 to 80 mV from a holding potential of –60 mV, as illustrated in Figure 1. This current gradually increased in size, typically stabilizing 6 to 20 minutes following cell break-in. This result was observed in most of the differentiating epithelial and fiber cells that we tested, although the amplitude of the current was variable and did not show a clear correlation to cell length/capacitance. In contrast, cells dialyzed with calcium-free internal solution displayed very small outward currents that did not increase over time. These findings indicate that the outwardly rectifying currents require calcium for activation.

Ion substitution experiments were performed to characterize the selectivity of the calcium-activated current for cations and anions. The reversal potential of the calcium-activated current was determined using the ramp protocol as the potential at which ramp-evoked currents intersected, as illustrated in Figure 2. When the fiber cells were bathed in standard external solution and the internal solution contained CsCl, the reversal potential of the calcium-activated current occurred at -3.17 ± 0.36 mV ($n = 14$), indicating that the calcium-activated current was either a nonspecific cation current or an anion current. To distinguish between these two possibilities, we replaced Na and Cs with NMDG in the bath solution and found that this had little or no effect on the reversal potential ($n = 7$). In contrast, substitution of 140 mM of the extracellular chloride with gluconate caused a positive shift in the reversal potential to 51.6 ± 3.31 mV ($n = 4$), which is close to the reversal potential for a perfectly selective chloride channel. These results indicate that the calcium-activated current is carried primarily by anions and has the permeability sequence: $Cl^- >>$ gluconate.

Figure 3A shows families of current traces recorded in response to depolarizing voltage clamp steps between –60 and 80 mV from a holding potential of –60 mV. In the presence of calcium-free internal solution, only very small currents were observed. At 200 nM $[Ca^{2+}]_i$, depolarizing voltage clamp steps evoked a slowly activating current that reversed polarity from inward to outward at ~0 mV. On repolarization to –60 mV, a large inward tail current was observed that slowly deactivated over time. The current-voltage (I-V) relationship measured at the end of the voltage clamp steps exhibited a significant degree of outward rectification (Fig. 3B). Further increases in $[Ca^{2+}]_i$ produced larger currents with less pronounced outward rectification. To quantify the degree of outward rectification, we determined the rectification index, calculated as the ratio of current measured in response to a 1 s voltage

Investigative Ophthalmology & Visual Science

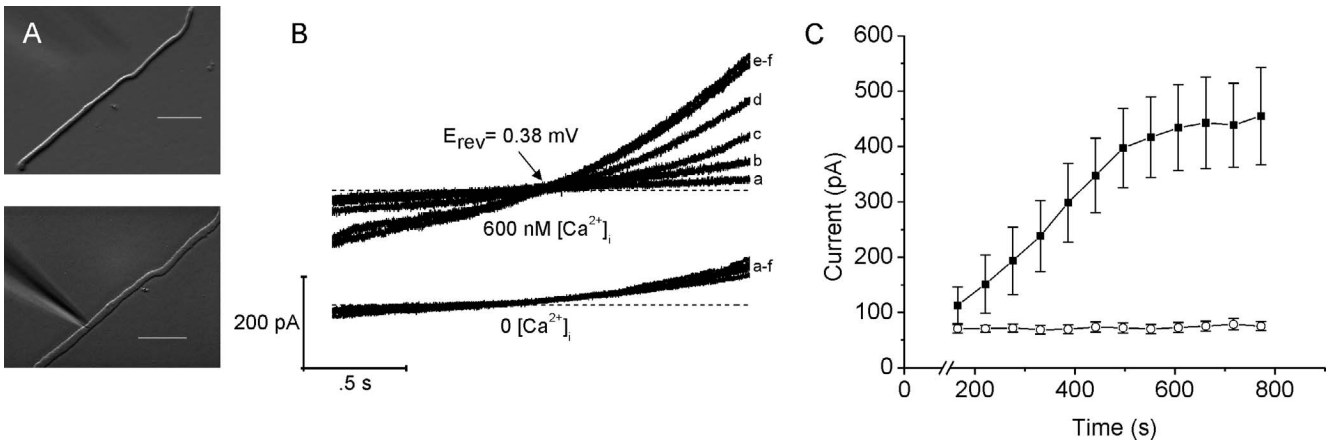

Figure 1. Mouse fiber cells express calcium-activated currents. (**A**) Image of a long fiber cell ~266 µm in length used in the patch clamp experiments before (*upper panel*) and 30 minutes after establishing a whole-cell patch (*lower panel*). *Scale bar*: 50 µm. (**B**) Experiment showing the time course of development of calcium-activated currents in a fiber cell during whole-cell dialysis. Whole-cell currents were measured in response to 2 s voltage clamp ramps from −80 to 80 mV from a holding potential of −60 mV. Bath solution contained (in mM) 140 NaCl, 10 CsCl, 4.7 KCl, 2 $MgCl_2$, 5 glucose, 5 HEPES (pH 7.4); patch pipette contained CsCl internal solution to which different calcium concentrations were added to give a final free calcium concentration of nominally zero and 600 nM. Ramp currents labeled a to f were recorded 110, 386, 441, 496, 607, and 662 s following patch rupture, respectively. Calcium concentration in the pipette is as indicated. *Dashed line* represents zero current. *Arrow* indicates the reversal potential of the calcium-sensitive current. (**C**) Plot of the time course of current activation at 80 mV as a function of time following patch rupture in the presence of 600 nM $[Ca^{2+}]_i$ (*closed squares*, $n = 6$) or nominally zero $[Ca^{2+}]_i$ (*open circles*, $n = 5$). Data are means ± SEM.

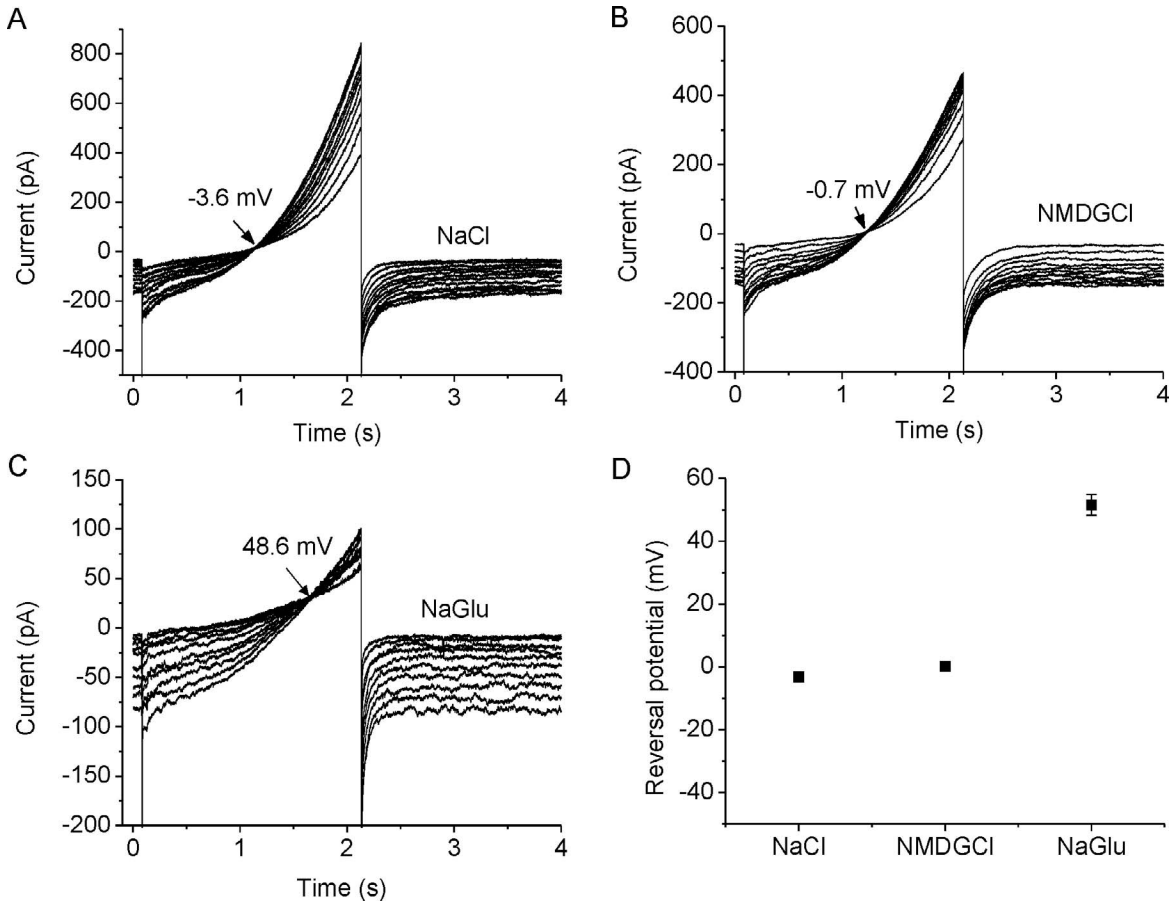

Figure 2. Ionic selectivity of the calcium-activated current in fiber cells. (**A**) Whole-cell currents measured in response to 2 s voltage clamp ramps from −80 to 80 mV from a holding potential of −60 mV. The pipette solution contained 600 nM $[Ca^{2+}]_i$. The bath solution contained NaCl (**A**), NMDG-Cl (**B**), or sodium gluconate (**C**) external solution. Ramp currents were recorded once every 55 s following patch rupture. The voltage at which the ramp currents intersected was taken to be the reversal potential of the calcium-activated current. (**D**) Graph summarizing the reversal potentials measured in the presence of the indicated bath solutions. Data are means ± SEM.

Investigative Ophthalmology & Visual Science

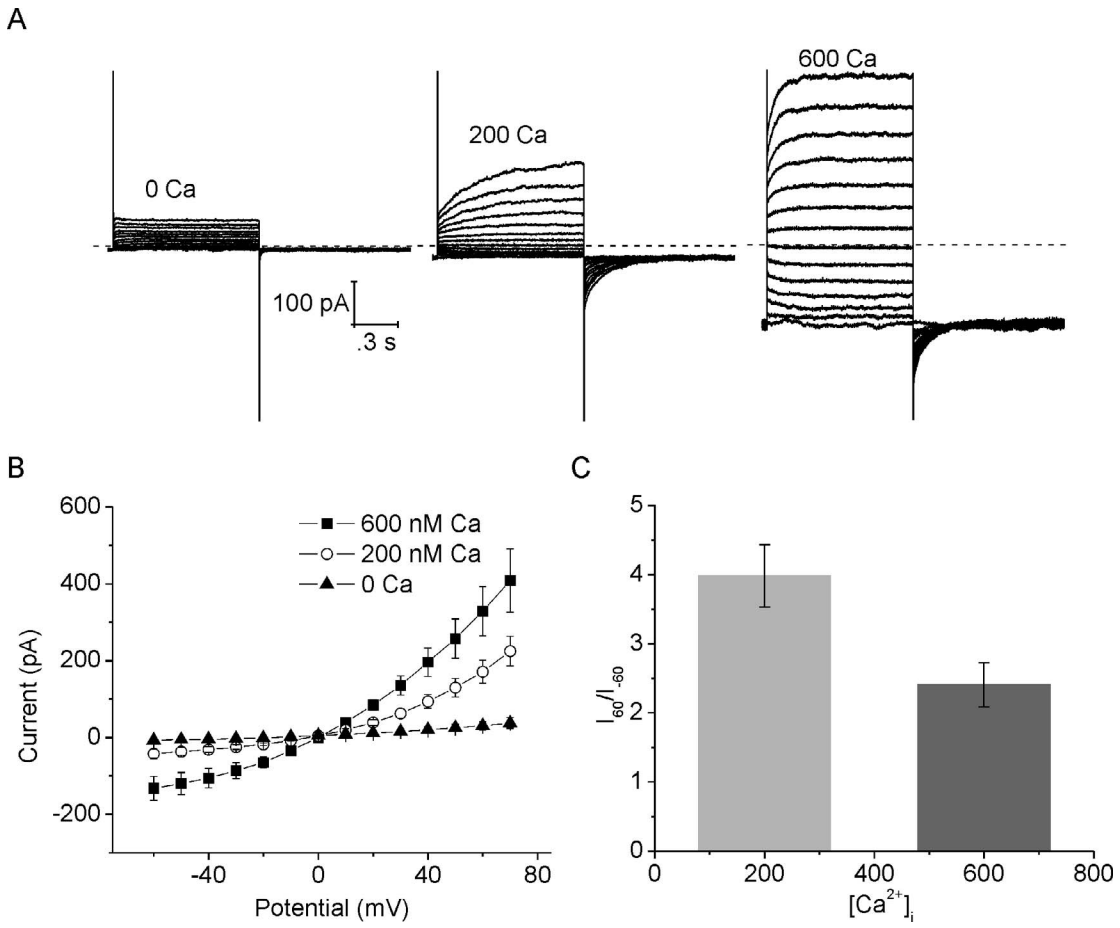

Figure 3. Effect of internal calcium on the calcium-activated current. (**A**) Families of whole-cell currents recorded from lens fiber cells in the presence of the indicated $[Ca^{2+}]_i$. The voltage clamp protocol consisted of sequential steps from a holding potential of –60 mV to 80 mV in 10-mV increments. *Dashed line* represents zero current. (**B**) I-V relationship (measured at the end of the pulse) in the presence of nominally zero $[Ca^{2+}]_i$ (*closed triangles*, $n = 6$), 200 nM $[Ca^{2+}]_i$ (*open circles*, $n = 4$), or 600 nM $[Ca^{2+}]_I$ (*closed squares*, $n = 3$). (**C**) Bar graph showing the mean rectification index determined as the ratio between the quasi steady-state current recorded in response to voltage clamp steps to +60 mV and the holding current at –60 mV. Data are means ± SEM.

clamp step to +60 mV to the holding current at –60 mV (Fig. 3C). The rectification index was 3.98 ± 0.45 ($n = 4$) at 200 nM $[Ca^{2+}]_I$ but only 2.4 ± 0.32 ($n = 3$) ($P < 0.05$) at 600 nM $[Ca^{2+}]_i$.

The calcium-activated chloride currents observed in response to depolarizing voltage clamp steps had 2 components: an instantaneous, time-independent component that represented channels that were open at the holding potential of –60 mV, followed by a time-dependent component that was due to channels that were activated by the voltage step. The time-dependent component could be described by a monoexponential function with a time constant of activation, τ_{act}. At 70 mV in the presence of 200 nM $[Ca^{2+}]_i$, τ_{act} was 266.63 ± 14.95 ms ($n = 3$), while at 600 nM $[Ca^{2+}]_i$, τ_{act} decreased to 104.46 ± 21.05 ms ($n = 3$). The time course of the tail currents observed following repolarization to –60 mV after a depolarizing voltage clamp step to 60 mV could also be described by a monoexponential function. The time constant of deactivation τ_{deact} was 123.10 ± 10.97 ms ($n = 3$) at 200 nM $[Ca^{2+}]_i$ and 100.95 ± 6.04 ($n = 3$) at 600 nM $[Ca^{2+}]_i$.

Pharmacological Properties of CaCCs in Fiber Cells

We investigated the effect of two second-generation compounds that have been reported to be potent blockers of TMEM16 CaCCs: CaCCinh-A01[10] and Ani9.[11] Figure 4A shows the effect of 50 μM CaCCinh-A01 on calcium-activated chloride currents in a fiber cell. CaCCinh-A01 strongly inhibited the calcium-activated chloride current at both positive and negative potentials. This inhibition was partially reversed following washout of blocker.

One problem with CaCCinh-A01 is that it cannot discriminate between TMEM16A and TMEM16B.[11,12] Therefore, we tested another novel CaCC inhibitor, Ani9, which has been reported to be a highly potent and selective blocker of TMEM16A with negligible effect on TMEM16B.[11] We observed that application of 5 μM Ani9 caused a reversible block of the calcium-activated chloride current that was similar to the effect of CaCCinh-A01, indicating that TMEM16A contributes to CaCCs in lens fiber cells (Fig. 4B). Figure 4C summarizes the percentage of current that was inhibited relative to the control current at –70 mV and +70 mV for CaCCinh-A01 and Ani9.

Expression of TMEM16A and TMEM16B in the Postnatal Mouse Lenses

The voltage gating properties, selectivity, and pharmacology of the calcium-activated current expressed in the differentiating, peripheral fiber cells closely resembled those of the classical calcium-activated chloride currents attributed to TMEM16A and TMEM16B.[13] Therefore, we used RT-PCR to assess the

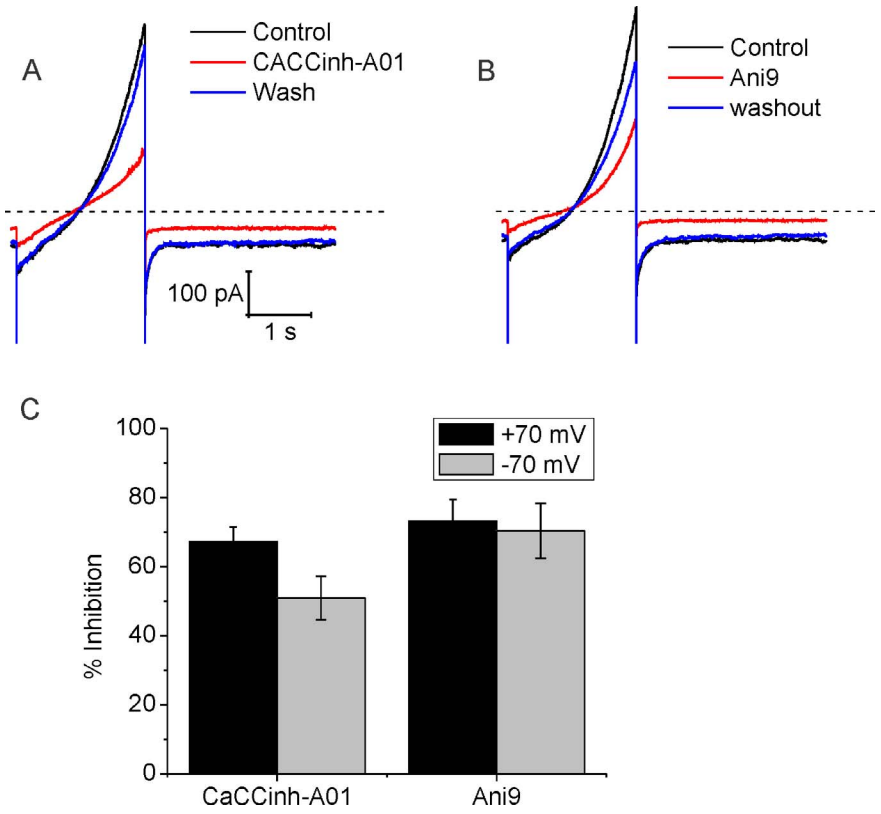

Figure 4. Effect of calcium-activated chloride channel blockers on the calcium-activated current. (**A**) Whole-cell currents measured in response to 2 s voltage clamp ramps from −80 to 80 mV from a holding potential of −60 mV. The pipette solution contained 600 nM $[Ca^{2+}]_i$. Ramp currents were measured first under control conditions (*black line*), then in the presence of 50 μM CACCinh-A01 (*red line*), and finally following washout of CACCinh-A01 (*blue line*). (**B**) Effect of Ani9 on the calcium-activated current in fiber cells. Whole-cell currents measured in response to 2 s voltage clamp ramps from −80 to 80 mV from a holding potential of −60 mV. The pipette solution contained 600 nM $[Ca^{2+}]_i$. Ramp currents were measured first under control conditions (*black line*), then in 5 μM Ani9 (*red line*), and finally following washout of Ani9 (*blue line*). (**C**) Percent of the current inhibited after treatment with 50 μM CaCCinh-A01 or 5 μM Ani9 at +70 and −70 mV. Data represent means ± SEM ($n = 4$).

expression of TMEM16A/B in mouse lenses. These studies demonstrate the presence of both TMEM16A and TMEM16B in wild-type and double KO mouse lenses (Fig. 5).

The distribution of TMEM16A/B proteins was mapped by immunohistochemistry. In axial sections of 10- to 14-day-old postnatal wild-type mouse lenses, TMEM16A expression was detected primarily in the epithelial cells and superficial, differentiating fiber cells near the equator of the lens (Figs. 6A–C). The most intense staining occurred in the newly elongating fiber cells whose apical ends form the modiolus.[14] Higher magnification images showed that the pattern of TMEM16A immunostaining appears to be both membranous and cytoplasmic in the newly elongating fiber cells, as shown in Figures 6D–F. In the adjacent epithelial cells and deeper layers of differentiating fiber cells, the staining pattern was mostly cytoplasmic. The localization of TMEM16A staining to the plasma membranes of the newly elongating fiber cells could be more clearly seen in equatorial sections through the modiolus (Figs. 6G–I). A similar pattern of TMEM16A staining was obtained using two other anti-TMEM16A polyclonal antibodies (data not shown).

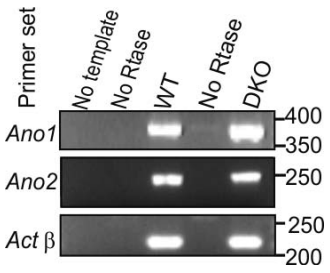

Figure 5. Reverse transcriptase-polymerase chain reaction (RT-PCR) analysis of TMEM16A and TMEM16B in wild-type and KO mouse lenses. β-actin was used as a control for cDNA integrity.

TMEM16B was also expressed primarily in the differentiating epithelial cells and newly elongating fiber cells near the equator of the lens (Figs. 7A–C). However, there were differences in the pattern of subcellular localization. Unlike TMEM16A, TMEM16B staining was principally membrane associated, except for a region of strong cytoplasmic labeling in the basal regions of the differentiating epithelium and newly elongating fibers at the periphery of the lens (Figs. 7D–F).

Discussion

In the present study, we demonstrate, for the first time, the functional expression of CaCCs in freshly isolated differentiating mouse lens fiber cells. These CaCCs generate currents with slow kinetics of activation and deactivation at $[Ca^{2+}]_I$ of ≥200 nM that are more similar to those of TMEM16A than TMEM16B expressed in heterologous expression systems. This result suggests that they are at least partially composed of TMEM16A.[15–18] Furthermore, pharmacologic studies using the highly potent and selective TMEM16A inhibitor Ani9[11] showed that application of 5 μM Ani9 strongly blocked CaCCs in lens

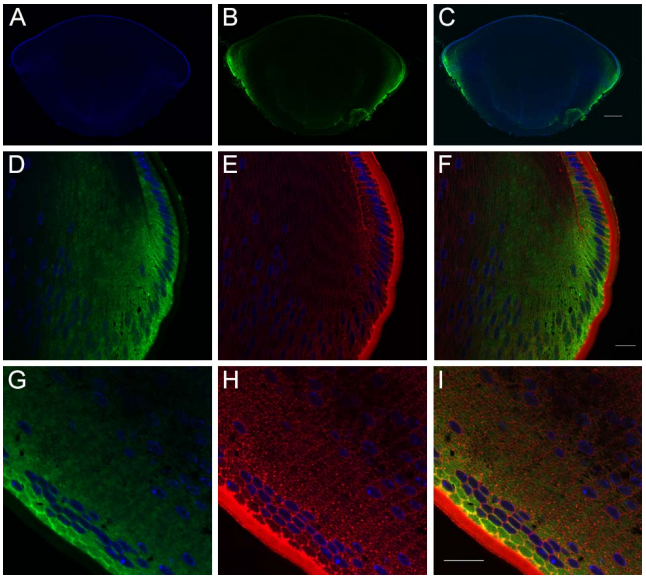

Figure 6. Distribution of immunoreactive TMEM16A is restricted to a superficial region around the equator of the lens. (**A–C**) Low-magnification images show the distribution of TMEM16A immunoreactivity (ab-72984; Abcam) in axial sections from 10-day-old wild-type mouse lenses. The localization of nuclei (*blue*) and TMEM16A (*green*) is shown either alone (**A** and **B**, respectively) or in combination (**C**). *Scale bar*: 150 µm. Images are representative of results from >3 animals. (**D–F**) Higher magnification confocal images of the epithelial cells and superficial newly elongating fiber cells near the equator in an axial section. The localization of TMEM16A (*green*) and the membrane marker WGA (*red*) is shown either alone (**D** and **E**, respectively) or merged (**F**). Nuclei are labeled with 4′,6-diamidino-2-phenylindole (DAPI; *blue*) in all panels. *Scale bar*: 20 µm. (**G–I**). Equatorial sections through the modiolus labeled with TMEM16A (*green*; **G**), WGA (*red*; **H**) alone, or merged (**I**). Nuclei are labeled with DAPI (*blue*) in all panels. *Scale bar*: 20 µm. Images are representative of results from >3 animals. Rabbit IgG isotype control experiments showed no signal (data not shown).

fiber cells, supporting our contention that TMEM16A channels contribute to CaCCs in lens fiber cells. It should be noted that interpretation of the electrophysiologic data is complicated by the existence of multiple splice variants of TMEM16A and TMEM16B that show differences in electrophysiologic properties. For example, the ac splice variant of human TMEM16A that skips segment b[10] has been reported previously to confer high calcium sensitivity on human and mouse TMEM16A in heterologous expression systems.[15,19] Furthermore, it has been reported that TMEM16A and TMEM16B can form heteromeric channels that have novel functional properties in both native tissues and heterologous expression systems.[20]

Using RT-PCR, we demonstrated that TMEM16A and TMEM16B transcripts are present in the postnatal mouse lens. Immunohistochemic mapping studies showed that TMEM16A and TMEM16B had a similar spatial distribution in the lens. Both proteins were present at highest levels in the differentiating epithelial cells and newly elongating fiber cells near the equator. As the fiber cells became more internalized within the lens, the signal intensity for these proteins decreased. The distribution of TMEM16A protein reported here is consistent with the findings of a lone previous in situ hybridization study that reported TMEM16A transcripts at high levels in the lens epithelium of the embryonic day 18.5 mouse eye.[21] Interestingly, a large fraction of the TMEM16A channels were present as a cytoplasmic pool within the newly elongating fiber cells. It is conceivable that these channels would be dynamically redistributed to the plasma membrane in response to mechanic

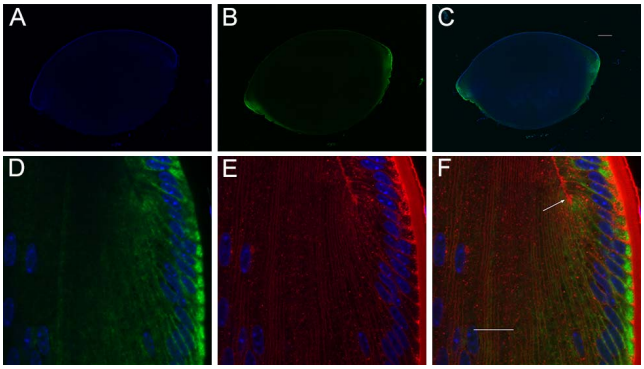

Figure 7. The expression pattern of TMEM16B partially overlaps that of TMEM16A in the lens. (**A–C**) Low magnification images show the distribution of TMEM16B immunoreactivity in axial sections from 10-day-old wild-type mouse lenses. The localization of nuclei (*blue*) and TMEM16B (*green*) is shown either alone (**A** and **B**, respectively) or in combination (**C**). *Scale bar*: 150 µm. Images are representative of results from >3 animals. (**D–F**) Higher magnification confocal images of the epithelial cells and superficial newly elongating fiber cells near the equator in an axial section from a 10-day-old wild-type mouse lens. The localization of TMEM16B (*green*) and the membrane marker WGA (*red*) is shown either alone (**D** and **E**, respectively) or merged (**F**). Nuclei are labeled with DAPI (*blue*) in all panels. *Arrowhead* indicates modiolus. *Scale bar*: 20 µm. Images are representative of results from >3 animals. Rabbit IgG isotype control experiments showed no signal (data not shown).

stress or changes in lens volume, as has been previously reported to occur for P2X receptors in the lens.[22] Taken together, our electrophysiologic and cell biologic studies suggest that native lens Ca^{2+}-activated Cl^- channels are made up of homomeric and/or heteromeric channels composed of TMEM16A and TMEM16B.

Physiologic Role of CaCCs in the Lens

The localization of TMEM16A/B CaCCs to the membranes of the newly elongating fiber cells near the surface of the lens makes them an ideal gate keeper for controlling water flow through the lens. One possible mechanism for water transfer involves the movement of chloride ions. The basic idea is that chloride ions from the aqueous humor surrounding the lens flow into the lens through extracellular spaces, enter the fiber cells via chloride transporters/channels, move between fiber cells via gap junctions, and then exit the lens fiber cells via peripheral CaCCs. This flow mechanism would add to flows related to sodium ions, as proposed in previous models.[1]

The existence of this flow mechanism is supported by experimentally observed changes in intracellular voltage from approximately –40 mV at the center of the lens to –60 mV at the surface of the lens.[23] Based on the generally assumed equilibrium potential of –50 mV for chloride in lens fiber cells, this would produce chloride influx near the center of the lens and chloride efflux at the periphery. In this scenario, changes in the opening probability of CaCCs in surface cells would be predicted to moderate this flow of chloride ions and accompanying water molecules through the lens.

This viewpoint is further supported by the current studies that suggest CaCCs in fiber cells reside mostly in the closed state at negative potentials in the presence of physiological levels of intracellular free calcium. However, increasing $[Ca^{2+}]_i$ to values of ≥200 nM caused a significant increase in CaCC activity. There are a number of ion channels and receptors in the lens epithelial cells and newly elongating fiber cells whose activation could trigger such an increase in intracellular

calcium and potentially result in the opening of CaCCs. These include TRPV1 and TRPV4 channels,[24–27] connexin and pannexin hemichannels,[5,25] and P2Y receptors.[28] Many of these channels and receptors have been reported to be involved in the activation of CaCCs in other types of cells.[29–33]

One situation in which these chloride fluxes mediated by CaCCs could play an important role is in volume regulation and in maintaining the spatial gradient in the index of refraction in the lens. It has been proposed previously that TRPV1 and TRPV4 act as sensors to detect changes in hydrostatic pressure at the surface of the lens. TRPV4 is activated by hypoosmotic solution and sends signals to increase the rate of water efflux from the lens by increasing the activity of the sodium/potassium ATPase in the lens epithelial cells. In contrast, TRPV1 is activated by hyperosmotic solutions and sends signals to decrease the rate of water efflux by either increasing the activity of NaKCC1 and/or inhibiting the sodium/potassium ATPase.[24,34,35] This, in turn, would return the hydrostatic pressure at the surface of the lens back to zero and, thus, maintain the normal gradient of water within the lens. Potentially, TMEM16A/B would also be an important part of this negative feedback control system. It would be interesting to determine whether TRPV4 and/or TRPV1 colocalizes with TMEM16A/B in the newly elongating lens fiber cells.

Another situation in which chloride and water flow mediated by CaCCs may be important is during accommodation. During deaccommodation, we propose that there is a flow of water from the deeper fiber cells to more peripheral fiber cells through gap junctions, followed by flow out of the lens (as reported for the bovine lens[36]). Egress of fluid from the lens would be mediated by mechanical distention of the surface cells that would trigger an increase in $[Ca^{2+}]_I$ via TRPV4 channels (or some other mechanism), an opening of CaCCs, chloride efflux, reduction in intracellular osmolarity, and movement of fluid out of the lens. Outflow of fluid appears to be concentrated near the equatorial surface of the lens based on the increased numbers of gap junctions and CaCCs near the equator.[37,38] Further experiments are needed to test this hypothesis and determine how it might complement other notions of accommodation.

Acknowledgments

The authors thank Yegor Korzyukov and Aditi Singh for their participation in the early phases of this project.

Supported by funding from National Institute of Health-NEI Grant R01EY026902 (LE).

Disclosure: **J.-J. Tong**, None; **P. Acharya**, None; **L. Ebihara**, None

References

1. Mathias RT, Kistler J, Donaldson P. The lens circulation. *J Membr Biol*. 2007;216:1–16.
2. Gao J, Sun X, Moore LC, Brink PR, White TW, Mathias RT. The effect of size and species on lens intracellular hydrostatic pressure. *Invest Ophthalmol Vis Sci*. 2013;54:183–192.
3. Webb KF, Donaldson PJ. Differentiation-dependent changes in the membrane properties of fiber cells isolated from the rat lens. *Am J Physiol Cell Physiol*. 2008;294:C1133–C1145.
4. Tunstall MJ, Eckert R, Donaldson P, Kistler J. Localised fibre cell swelling characteristic of diabetic cataract can be induced in normal rat lens using the chloride channel blocker 5-nitro-2-(3-phenylpropylamino) benzoic acid. *Ophthalmic Res*. 1999;31:317–320.
5. Ebihara L, Tong J-J, Vertel B, White TW, Chen TL. Properties of connexin 46 hemichannels in dissociated lens fiber cells. *Invest Ophthalmol Vis Sci*. 2011;52:882–889.
6. Ebihara L, Korzyukov Y, Kothari S, Tong J-J. Cx46 hemichannels contribute to the sodium leak conductance in lens fiber cells. *Am J Physiol Cell Physiol*. 2014;306:C506–C513.
7. Wang E, Geng A, Maniar AM, Mui BW, Gong X. Connexin 50 regulates surface ball-and-socket structures and fiber cell organization. *Invest Ophthalmol Vis Sci*. 2016;57:3039–3046.
8. Hu Z, Shi W, Riquelme MA, et al. Connexin 50 functions as an adhesive molecule and promotes lens cell differentiation. *Sci Rep*. 2017;7:5298.
9. Kamikawa A, Ichii O, Sakazaki J, Ishikawa T. Ca2+-activated Cl- channel currents in mammary secretory cells from lactating mouse. *Am J Physiol Cell Physiol*. 2016;311:C808–C819.
10. De La Fuente R, Namkung W, Mills A, Verkman AS. Small-molecule screen identifies inhibitors of a human intestinal calcium-activated chloride channel. *Mol Pharmacol*. 2008;73:758–768.
11. Seo Y, Lee HK, Park J, et al. Ani9, A novel potent small-molecule ANO1 inhibitor with negligible effect on ANO2. *PLoS One*. 2016;11:e0155771.
12. Namkung W, Phuan PW, Verkman AS. TMEM16A inhibitors reveal TMEM16A as a minor component of calcium-activated chloride channel conductance in airway and intestinal epithelial cells. *J Biol Chem*. 2011;286:2365–2374.
13. Scudieri P, Sondo E, Ferrera L, Galietta LJ. The anoctamin family: TMEM16A and TMEM16B as calcium-activated chloride channels. *Exp Physiol*. 2012;97:177–183.
14. Zampighi GA, Eskandari S, Kreman M. Epithelial organization of the mammalian lens. *Exp Eye Res*. 2000;71:415–435.
15. Ferrera L, Caputo A, Ubby I, et al. Regulation of TMEM16A chloride channel properties by alternative splicing. *J Biol Chem*. 2009;284:33360–33368.
16. Yang YD, Cho H, Koo JY, et al. TMEM16A confers receptor-activated calcium-dependent chloride conductance. *Nature*. 2008;455:1210–1215.
17. Stephan AB, Shum EY, Hirsh S, Cygnar KD, Reisert J, Zhao H. ANO2 is the cilial calcium-activated chloride channel that may mediate olfactory amplification. *Proc Natl Acad Sci U S A*. 2009;106:11776–11781.
18. Pifferi S, Dibattista M, Menini A. TMEM16B induces chloride currents activated by calcium in mammalian cells. *Pflugers Arch*. 2009;458:1023–1038.
19. Sung TS, O'Driscoll K, Zheng H, et al. Influence of intracellular Ca2+ and alternative splicing on the pharmacological profile of ANO1 channels. *Am J Physiol Cell Physiol*. 2016;311:C437–C451.
20. Yamamura H, Nishimura K, Hagihara Y, Suzuki Y, Imaizumi Y. TMEM16A and TMEM16B channel proteins generate Ca(2+)-activated Cl(–) current and regulate melatonin secretion in rat pineal glands. *J Biol Chem*. 2018;293:995–1006.
21. Gritli-Linde A, Vaziri SF, Rock JR, et al. Expression patterns of the Tmem16 gene family during cephalic development in the mouse. *Gene Expr Patterns*. 2009;9:178–191.
22. Suzuki-Kerr H, Lim JC, Vlajkovic SM, Donaldson PJ. Differential membrane redistribution of P2X receptor isoforms in response to osmotic and hyperglycemic stress in the rat lens. *Histochem Cell Biol*. 2009;131:667–680.
23. Gao J, Wang H, Sun X, et al. The effects of age on lens transport. *Invest Ophthalmol Vis Sci*. 2013;54:7174–7187.
24. Mandal A, Shahidullah M, Delamere NA. TRPV1-dependent ERK1/2 activation in porcine lens epithelium. *Exp Eye Res*. 2018;172:128–136.
25. Shahidullah M, Mandal A, Delamere NA. TRPV4 in porcine lens epithelium regulates hemichannel-mediated ATP release and Na-K-ATPase activity. *Am J Physiol Cell Physiol*. 2012;302:C1751–C1761.

26. Shahidullah M, Mandal A, Beimgraben C, Delamere NA. Hyposmotic stress causes ATP release and stimulates Na,K-ATPase activity in porcine lens. *J Cell Physiol*. 2012;227:1428–1437.
27. Martinez-Garcia MC, Martinez T, Paneda C, Gallego P, Jimenez AI, Merayo J. Differential expression and localization of transient receptor potential vanilloid 1 in rabbit and human eyes. *Histol Histopathol*. 2013;28:1507–1516.
28. Hu RG, Suzuki-Kerr H, Webb KF, et al. Molecular and functional mapping of regional differences in P2Y receptor expression in the rat lens. *Exp Eye Res*. 2008;87:137–146.
29. Dutta AK, Woo K, Khimji AK, Kresge C, Feranchak AP. Mechanosensitive Cl– secretion in biliary epithelium mediated through TMEM16A. *Am J Physiol Gastrointest Liver Physiol*. 2013;304:G87–G98.
30. Cherkashin AP, Kolesnikova AS, Tarasov MV, et al. Expression of calcium-activated chloride channels Ano1 and Ano2 in mouse taste cells. *Pflugers Arch*. 2016;468:305–319.
31. Derouiche S, Takayama Y, Murakami M, Tominaga M. TRPV4 heats up ANO1-dependent exocrine gland fluid secretion. *FASEB J*. 2018;32:1841–1854.
32. Takayama Y, Uta D, Furue H, Tominaga M. Pain-enhancing mechanism through interaction between TRPV1 and anoctamin 1 in sensory neurons. *Proc Natl Acad Sci U S A*. 2015;112:5213–5218.
33. Takayama Y, Shibasaki K, Suzuki Y, Yamanaka A, Tominaga M. Modulation of water efflux through functional interaction between TRPV4 and TMEM16A/anoctamin 1. *FASEB J*. 2014;28:2238–2248.
34. Gao J, Sun X, White TW, Delamere NA, Mathias RT. Feedback regulation of intracellular hydrostatic pressure in surface cells of the lens. *Biophys J*. 2015;109:1830–1839.
35. Shahidullah M, Mandal A, Delamere NA. Activation of TRPV1 channels leads to stimulation of NKCC1 cotransport in the lens. *Am J Physiol Cell Physiol*. 2018;315:C793–C802.
36. Gerometta R, Zamudio AC, Escobar DP, Candia OA. Volume change of the ocular lens during accommodation. *Am J Physiol Cell Physiol*. 2007;293:C797–C804.
37. Baldo GJ, Mathias RT. Spatial variations in membrane properties in the intact rat lens. *Biophys J*. 1992;63:518–529.
38. Boswell BA, Le AC, Musil LS. Upregulation and maintenance of gap junctional communication in lens cells. *Exp Eye Res*. 2009;88:919–927.

Investigative Ophthalmology & Visual Science